CONF-850953--23

UCRL--92437

DE87 008159

UCRL- 92437
PREPRINT

Received by OSTI

MAY 0 4 1987

THE ROLE OF CALCULATIONS TO DEFINE CONTAINMENT PHENOMENOLOGY IN COMPLEX GEOLOGY

Robert P. Swift
John T. Rambo
Jon B. Bryan

This Paper Was Prepared for Submittal to
Third Containment Symposium
Idaho Falls, Idaho
September 9-13, 1985

October 1985

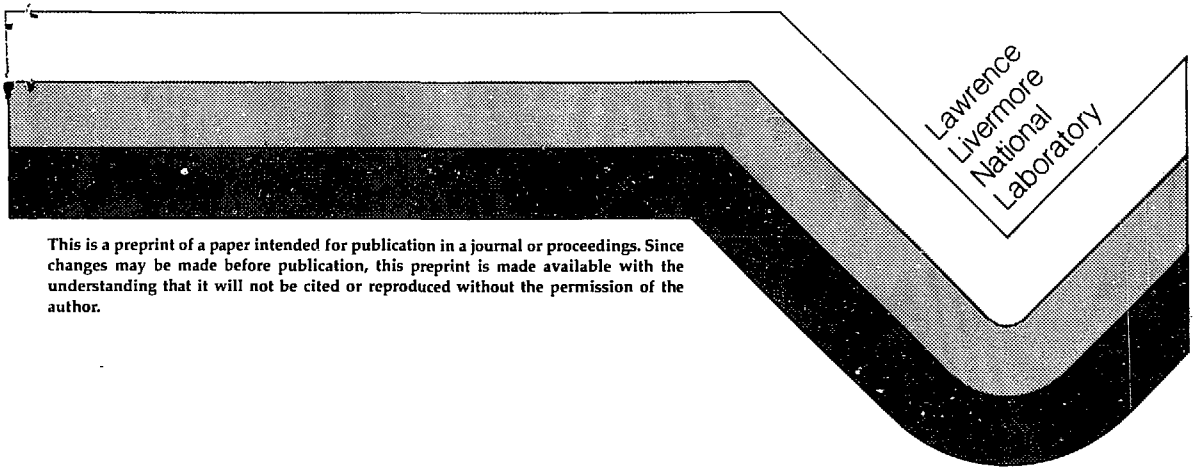

This is a preprint of a paper intended for publication in a journal or proceedings. Since changes may be made before publication, this preprint is made available with the understanding that it will not be cited or reproduced without the permission of the author.

DISTRIBUTION OF THIS DOCUMENT IS UNLIMITED

DISCLAIMER

This document was prepared as an account of work sponsored by an agency of the United States Government. Neither the United States Government nor the University of California nor any of their employees, makes any warranty, express or implied, or assumes any legal liability or responsibility for the accuracy, completeness, or usefulness of any information, apparatus, product, or process disclosed, or represents that its use would not infringe privately owned rights. Reference herein to any specific commercial products, process, or service by trade name, trademark, manufacturer, or otherwise, does not necessarily constitute or imply its endorsement, recommendation, or favoring by the United States Government or the University of California. The views and opinions of authors expressed herein do not necessarily state or reflect those of the United States Government or the University of California, and shall not be used for advertising or product endorsement purposes.

THE ROLE OF CALCULATIONS TO DEFINE CONTAINMENT PHENOMENOLOGY IN COMPLEX GEOLOGY

Robert P. Swift
John T. Rambo
Jon B. Bryan

ABSTRACT

Containment evaluation of some underground nuclear events has become strongly dependent on the use of calculations to help define important phenomenology. This results from the increasing necessity to test in sites having a geology that precludes acceptance based solely on experience. This paper discusses the rationale of a suite of TENSOR code calculations undertaken in support of the containment evaluation for a recent event and highlights the results of these calculations. The calculations illustrate containment phenomena in a layered geology of alluvium and tuff with a working point in the proximity of the Paleozoic surface. They show that reflected disturbances from surfaces above and/or below the working point can significantly hinder the development of the residual stress field if their arrival in the residual stress region coincides with the rebound phase of cavity growth. In addition, the results demonstrate a need for the development of a criterion for the probability of successful containment in complex geology other than the historical concept of a strong, sufficiently thick residual stress field.

INTRODUCTION

As the U.S. underground nuclear testing continues at the Nevada Test Site, the availability of site geologies that are well understood will decrease. This scarcity of real estate increases the chance of future tests having test conditions coupled with site geologies that preclude containment acceptance based solely on experience from past events. Under such circumstances a need

MASTER

EGB

DISTRIBUTION OF THIS DOCUMENT IS UNLIMITED

exists to rely more heavily on other ways to evaluate containment, including the use of numerical code calculations to simulate the phenomena associated with the containment of an event.

Calculations are often conducted to provide insight into expected phenomena for the containment evaluation process of underground nuclear events. They are more frequently used for events where unusual complex geologies are encountered, that are not well understood in a containment sense (i.e., conditions exist that are not confortably in the realm of experience), as opposed to events where the geologies are simple or typical of those that have successfully contained in the past. For the latter, calculations which we ascribe as successful containment are associated with the formation of a thick (i.e., one to two cavity radii) residual stress region with compressive stress components well above the cavity pressure. For the former, calculations often reveal the lack of a residual stress region or a highly degraded one. In this paper we discuss the rationale and highlight results of a suite of calculations performed with the TENSOR code [1] in support of the containment evaluation of an event in hole U8j having certain conditions marginally near the norm of experience.

The calculations discussed in this paper form a parametric set with respect to material strength and geology, as well as addressing specific site containment phenomenology. They illustrate containment phenomena in a layered geology of alluvium and tuff with a workpoint in the proximity of the Paleozoic surface. Specifically, they show that reflected disturbances from surfaces above and/or below the WP can greatly impair the development of residual stresses if their arrival in the residual stress region coincides with the rebound phase onset of cavity growth. The onset of rebound is strongly sensitive to material strength [2]. Hence, for a given geology, the strength of the WP material relative to the adjacent layers dictates the degree of influence that reflections will have on the residual stresses. In cases where the effect is significant a need exists for a criterion to provide the probability of successful containment other than the historical concept of a strong, sufficiently thick residual stress field. Calculations of the nature discussed here verified against field events and small scale phenomenological modeling experiments can help formulate a representative criterion. With this approach, it is anticipated that significant progress can be made with regard to the existing experience.

RATIONALE

In response to a request by the Containment Evaluation Panel (CEP), calculations were performed to assist in defining the containment phenomena for a test in hole U8j having the geology shown in Figure 1. The proximity of the paleozoic (PZ) surface to the working point (WP) for this event was a chief concern because of the potential strong reflection off the PZ surface back into the WP region. Also, the layers above the WP were more porous and weaker than the WP Fraction Tuff, which again could allow reflections (i.e., rarefactions) to propagate back into the WP region and affect the development of the residual stress field. In addition, a thin weak layer of colluvium (i.e., alluvium containing large amounts of clay) was indicated to exist just above the PZ surface. Recent laboratory experiments [3], using small spherical charges in rock grout simulant with a WP close to a granite interface, indicated a greater degradation to the resi- dual stress field when a thin layer of clay separated the grout from the harder granite than when the clay layer was absent. The geology of this event was only marginally in the domain of previous experience. Because of this and of the uncertainty of the effects of a close PZ, the weak layer above it, and the weak upper layers, the CEP felt it prudent to examine this event by calculations.

The physics associated with the development of a residual stress field for an underground explosion in an idealized nonlayered geology have been extensively studied [4-6]. Figure 2a shows the calculated residual out-of-plane hoop stress at a time of equilibrium for an explosion in nonlayered geology. For this case the residual stresses in the entire region surrounding the cavity are well above the cavity pressure. Reduction of the residual stresses can be caused by the arrival of disturbances. For example, reflections from the ground surface can alter the residual stress region, with considerable degradation if the depth-of-burial is too shallow. Furthermore, reflections from buried layers, especially those in close proximity to the working point, can also greatly influence the residual stresses as illustrated in Figure 2b. In general, there is a lack of understanding of how shock wave interaction with buried layers near the WP affects residual stresses and the containment of an event, although in some specific cases calculations have

been used to define plausible scenarios (e.g., calculations of the Baneberry event [7]). The problem is that each site is different; thus, for a given yield, the effects detrimental to the development of a good residual stress field are mutually dependent on geology and material properties in a temporal and spatial manner. This makes it very difficult to ascertain in a general sense whether or not containment is assured. The existence of a good residual stress field may be sufficient but not necessary for successful containment.

Calculations used in the decision making process in support of containment evaluations are usually based on the estimated worst combination (i.e., conservative) of geology and material properties. This provides a way to address potential problem areas that may be exposed by the calculated phenomena and, combined with previous knowledge and experience, allows for a more objective assessment of an event's containment prospects. However, when the complexity of the geology and the uncertainty of the material properties combined with device characteristics are outside the norm of experience it is difficult to make a conservative estimate of the computational model. This often necessitates several calculations to deduce phenomena and to unravel the influences of material properties from those of geology.

CALCULATIONAL APPROACH

Configuration

The calculations were performed using the TENSOR code [1]. This code uses an explicit finite difference two-dimensional Lagrangian scheme that integrates the conservation equations of continuum mechanics to solve stress wave propagation problems. TENSOR can model plane strain or axisymmetric geometries. For containment problems an axisymmetric configuration is normally employed with the axis of symmetry projected from the WP perpendicular to the ground surface. For the geology shown in Figure 1, the PZ surface is inclined about 18 degrees to the horizontal. Using the configuration described above, the PZ would act as a conical reflector focusing unrealistic reflections along the axis above the WP. To circumvent this unreal effect in the calculation, the axis of symmetry was made normal to the PZ surface. The configuration is

shown in Figure 3. Here it is noted now that the ground surface will act as a conical reflector. However, it is much further removed from the WP region and any reflections will be significantly weaker in comparison than those from the interior surfaces.

Calculational Suite

The suite of TENSOR calculations performed for the present study are shown in Figure 4. Certain calculations (COTTS, COTTG, COTTL) addressed the influence of the upper layers only while others (COTTT and COTTK) addressed the effects of the PZ and weak colluvial layer below the WP. The rest, with the exception of COTTU, combine the influence of upper and lower layers and pertain to the baseline geology. The solid lines connecting the boxes convey a route through the calculational matrix along which only one variation either in geology or strength has been made between the respective calculations. The case with uniform geology, COTTU, having no layering stands alone with the only commonality being the shear strength that is representative of the WP material. The shear strengths used in each case above the horizontal dashed line in Figure 4 were based on estimates from laboratory data, geophysical logging data, and experience from calculations of other events. Their values along with other material property values are discussed below. Variations from these strengths were used in the cases shown below the horizontal dashed line. This calculational matrix does not cover all combinations, but it does provide a good insight into the sensitivity of the residual stress field to changes in layering and strength for a specific geology. However, it is felt that future more complete computational studies should be based on simpler geological configurations.

Boundary Conditions

The TENSOR calculational mesh and dezoning procedure was the same for all calculations. The mesh consisted of 8280 zones including 60 L lines that radiate outward from the cavity and 138 K lines. The zero K-line and K-line 138 defined the cavity boundary and the outer boundary including the ground surface, respectively. Dezoning was carried out automatically based on information prescribed in a run control instruction file.

The calculations were carried out to 1.5 seconds when a state of equilibrium was well established. They were driven by a pressure-profile (P versus volume) boundary condition applied to the zero K-line cavity radius, R = 23.6 m. The pressure volume condition allows for the influence of reflections on the growth of the cavity. It was derived from spherical one-dimensional calculations performed with the same yield, layering, and material properties as used in the two-dimensional TENSOR calculations. The one-dimensional calculations used to generate the source cavity loading condition accounted for vaporization and melting with the source being modeled as an iron gas [8,9] having an initial radius of 0.98 m and density of 1.5 Mg/m^3.

Baseline Material Model

The constitutive models used in TENSOR calculations account for pore collapse, ductile and brittle shear failure, and tensile failure with crack opening and closure. In containment calculations the material parameter input is usually chosen to reflect some a-priori concepts of what could constitute a reasonable worst case combination of geologic factors and unmeasured material properties. The baseline calculation, COTTR, reflected three factors: 1) laboratory measurements of a high shear strength for the WP Fraction Tuff were assumed to be representative of the actual strength; 2) the interface regions were represented as sharp discontinuities with respect to material properties so as to cause greater reflections in the region of residual stress; and 3) significantly reduced residual stresses were indicated from small scale laboratory experiments [3] and were attributed to the presence of a thin weak layer separating the WP material from the strong PZ material. The measured strength data from samples of Fraction Tuff [10] are shown in Figure 5 along with the representation used in the baseline calculation. Table 1 gives the geophysical property values [11] used in the baseline calculation to generate compressibility and shear strength behavior for the various layers with the aid of the Butkovich model [8].

With respect to (1), the Fraction Tuff strength is possibly higher than that of other typical tuffs and alluvium found in Yucca Valley. This is indicated by the calculated equivalent shear strength index based on cavity radius using the scaling model developed in [2,12] for three events executed

in Fraction Tuff, see Table 2. These strengths are higher than the average Yucca strength which are about 3-10 MPa. The CEP K values for SHUFFLE and BILBY are low and may be the result of their proximity to the PZ resulting in smaller than normal cavity radius. The K value for FRISCO, a nearby Area 8 event, is close to the CEP average of 70.2. FRISCO was also simulated with TENSOR using the laboratory strength measured in Fraction Tuff at U8j. The resulting calculated cavity radius was within 2 percent of the measured value, again indicating that the measured shear strength shown in Figure 5 is possibly representative of the in-situ strength of fraction tuff for this region of Area 8.

With regard to (2) above, all the layers were modeled as having abrupt interfaces where different averaged material properties meet. The porous upper layers above the WP were assigned very low shear and elastic strength to maximize rarefactions from failed or crushed up material. This type of modeling would provide more severe rarefactions in the WP region from the high stress plastic wave at the interface [13]. The reflections induced below the WP from the PZ surface are modeled in the same manner that has been used in other calculations, such as BANEBERRY [7].

In regard to (3), there was a suggestion that the undifferentiated tuff layer just above the PZ might be weaker than the Fraction Tuff. The caliper log indicated a greater degree of caving in this region, although drilling rates did not show a significant change through that depth range. In addition, small scale HE experimental evidence indicated that a weak clay like interface along a stiff granite boundary could produce a reduction in residual stress [3]. Furthermore, 2-D simulations of the experiments indicated residual stress weakness, [14,15]. This weak interface was included in the baseline geology because of the perception from experiments and calculations that it was conservative to do so.

The complexity of the COTTR calculation required sensitivity calculations addressing geology and shear strength to better understand the different reflecting contributions degrading the residual stresses. The result of these sensitivity calculations are discussed in the following section.

CALCULATIONAL RESULTS AND DISCUSSION

The calculational results discussed here illustrate how the residual stresses are degraded by layering in close proximity (i.e., two cavity radii or less) to the WP. The results indicate that residual stress field degradation is dependent in a complicated way on the arrival and magnitude of reflections from the layers relative to the onset of rebound. Furthermore, the influence of the reflections are very sensitive to differences between strength in the WP region and that of the layers.

A summary of the calculational results are given in Table 3. As noted, the grouping is according to geology, and, in the groups where material strength variations were made, the results are ordered from the lowest to the highest strength. Included are the cavity pressure, the associated effective cavity radius, the onset time of horizontal rebound, and an indication of whether the in-plane tangential or out-of-plane hoop residual stresses are above, about the same, or below (i.e., high, marginal, low) the cavity pressure. Also, values are given of the strength of the residual stress region and of the onset time for rebound determined from the cube root scaling model in [2,12] using the yield, calculated cavity radius, and overburden pressure as input. Since the scaling model is based on the assumptions of uniform geology with a constant strength, the strength and onset rebound values represent index values for a particular configuration. These index values were included because they help indicate a trend of the residual stress field with respect to geology and strength variations. With the exception of COTTT, good agreement between the calculated and cube root scaling model equivalent onset times occur for a higher strength index, while the calculated times are notably longer for the cases of a low strength index. The longer time for COTTT is attributed to the weak colluvial layer on top of the PZ surface which has a delaying effect on rebound even though the strength index is fairly high.

Residual Stress Fields

The calculated residual stress fields described in Table 3 are ranked in an order ascending from the best field, COTTU, to the most degraded field, COTTS. This ranking is purely objective and is based on the observed

combination of tangential and hoop residual stress fields relative to cavity pressure. It is observed that the baseline case, COTTR, thought to be very conservative at the time it was calculated, has the fourth best overall residual stress field for the layered cases. However, the worst case results when only the upper layers having their baseline strengths are considered (i.e., COTTS). This indicates the action of reflections from the lower layering counteracts that from the upper layers. The best residual stress field for a layered case is obtained in COTTG which also has upper layers only and is achieved by increasing the COTTS baseline strength for the upper layers to be that of the WP material. Note that the strength index based on the cube root scaling model is increased by only 1 MPa from the worst case COTTS to the best case COTTG.

While a higher strength index is associated with a better residual stress field when upper layers only are involved, the opposite is observed for the case of lower layers (i.e. COTTT and COTTK) or when lower layering is combined with upper layering (i.e., COTTZ through COTTX). The only good residual stress field obtained for the cases combining upper and lower layers, without the thin colluvial layer atop the PZ, is achieved in COTTZ by reducing the WP strength to one-half its baseline value. Slightly increasing the strength to 5/8 of the baseline, COTTH, resulted in a low hoop stress. Furthermore, by removing the thin weak colluvial layer separating the WP and PZ materials we go from a fairly good residual stress field in COTTR to a very deteriorated one in COTTX. Here the colluvial layer has a large effect of about 22.5 percent on the strength index value.

Calculated residual stress results obtained in the baseline model, COTTR, are illustrated in Figure 6. Shown are isometric, contour, and profile plots of the in-plane tangential stress and out-of-plane hoop stress at a time of one second. The nonshaded area in the contour plots, Figures 6c and d, indicate the region where the residual stresses are above the cavity pressure. The profile plots, Figures 6e and f, show the stress distributions in the residual stress region around the outside of cavity from the bottom to the top (i.e., -90 to 90 degrees) at radii of 65, 70, and 80 meters. The cavity pressure is also shown. Overall, the tangential stress field is somewhat lower than the hoop stress field with the weaker regions being below the cavity from the vertical out to about 40 degrees and above the horizontal from about 30 to 60 degrees.

In order to illustrate the varying influence that reflections off different layers have on the resulting residual stress field, the effects of the lower layers are examined in Figure 7 for COTTT and, in contrast, the effects of the upper layers are examined in Figure 8 for COTTS. A significantly better residual stress field is observed for the lower layer case COTTT than for the upper layer case COTTS. The marginal area for COTTT is in the tangential stress in the horizontal region and below the cavity. The rarefaction off the upper layers in COTTS is much more severe causing both the tangential and hoop stresses along the horizontal above and slightly below the WP level to fall below the cavity pressure. When the effects of the upper and lower layers are combined, the severe degradation induced by the rarefaction from the upper layers is counteracted by that of the lower layers resulting in a fairly good residual stress field as seen in Figure 6 for COTTR.

The counteraction to the strong rarefaction from the upper layers is mainly due to the weak colluvial layer atop the PZ surface. Reducing the thickness of the colluvial layer (i.e., COTTW, with thickness 1/2 that of COTTR) results in lower residual stresses and total removal of this layer results in an extremely poor residual stress field as shown in Figure 9 for COTTX. Here the most severely affected is the hoop stress in the horizontal region above and below the WP. Without the weak colluvial layer, a 50 percent reduction in the strength of the WP material from its baseline level is required to establish a good residual stress field (i.e., case COTTZ). Note, from Table 3, this reduction in WP strength is manifested as a 38 percent reduction in the strength index. In contrast, when the upper layers only are involved, a good residual stress field results for about a 6 percent increase in the strength index (i.e., COTTG). These observations indicate the complexity of the interacting effects of layering and the sensitivity on strength. To better understand how degradation of the residual stress field occurs it is helpful to examine the non-radial motion in the residual stress region resulting from the arrival of reflections off the layers.

Non-Radial Motion

The interaction of an outgoing shock wave with layering around the WP causes reflections to be propagated back into the residual stress region. An illustration of this phenomenon is given in Figure 10. The reflections perturb the normal radial like motion in this region and induce a small amount of non-radial motion. If the non-radial motion occurs at a time near the onset of rebound, it can, depending on its amplitude, disrupt the normal radial rebound process and impede the subsequent development of residual stresses. Typical examples of non-radial motion are shown in Figure 11 in the form of vertical velocity at the WP depth and at a horizontal range of 50 m. The corresponding radial motion is superimposed and shown at its full scale in Figure 11a. In Figures 11b-f the scale is such as to emphasize the non-radial motion and the negative phase of the radial motion. For the nonlayered case, COTTU in Figure 11b, the non-radial motion is entirely due to the influence of overburden gradient on the rebound phase and is a common contribution for all cases. This is a marked contrast with the vertical motion caused by shock interaction with the layering in Figures 11c-f.

Initially, reflections tend either to reload or unload their area of influence, depending on the relative impedances of the layers involved. The initial arrival of the reflection at the WP level from lower layering is about 0.05 s, is compressive and causes a sharp upward vertical motion as seen in Figure 11c for COTTT. The initial arrival off the upper layering is about 0.07 s, rarefactive, and causes at first a more gradual upward vertical motion as seen in Figure 11d. The latter part of the vertical motion manifests the deformation character of the involved layers. For example, the sudden downward turn observed in Figure 11c for COTTT is a result of considerable compressing and shearing (i.e., extruding) of the weak colluvial layer between the harder WP Fraction Tuff and PZ material. This behavior is also evident, but to a less extent, for COTTR in Figure 11e where the downward tending motion is retarded by the strong counteracting rarefaction (i.e., see Figure 11d COTTS) off the weaker upper layering. The small upward increase in motion observed for COTTR in Figure 11e around 0.3 to 0.35 s is the contribution from the overburden gradient. The effect of the absence of a thin weak layer above the PZ surface is shown for COTTX in Figure 11f. Here the strong reflection off the PZ is

reinforced slightly later by the rarefaction from the upper layers. This leads to a much higher and broader non-radial pulse which results in considerable degradation of the residual stress field, as seen in Figure 9. Figure 12 shows that the non-radial motion occurring in COTTR is approximately composed of the contributing influences of upper layers in COTTS and lower layers in COTTT. Similarly, Figure 13 shows that the enhanced motion in COTTX is composed of the rarefaction from COTTS and the direct reflection off the PZ surface in COTTK when the buffering colluvial layer is removed.

As stated above, if the amplitude of reflection induced non-radial motion is sufficient and arrives near the time of rebound, the normal radial inward motion associated with lock-up is significantly impeded resulting in one or more components of the residual stresses being below the cavity pressure. Of the twelve cases considered six have residual stresses degraded below their cavity pressure, see Table 3. The calculations indicate that the degree of degradation varies considerably with geology and strength. The threshold non-radial motion capable of causing the tangential stress or hoop stress residual values to fall below the cavity pressure is sensitive to the geologic configuration, shear strength, and rebound time. This is shown in Table 4 which has the same grouping as described above for Table 3. The values shown for peak non-radial motion, time difference between the rebound onset and peak non-radial motion, and the additional non-radial displacement occurring after rebound onset are with respect to the WP depth and an initial horizontal range of 50 m. Values at other ranges and/or orientations in the residual stress field are slightly different but their trends are similar. Also, shown for completeness is the ranking of the residual stress fields.

Table 4 shows that the amplitudes of the non-radial motion and displacement after rebound onset vary according to the geologic groupings. The trend of non-radial motion among all the groupings is consistent with respect to its effect on residual stresses. Namely, the cases having low residual stresses are associated with the higher non-radial motions and displacements. The results in Tables 3 and 4 also indicate that a low residual stress field is more likely to occur if the peak non-radial motion is close to the rebound onset. For all cases considered except for those with upper layers only, a better residual stress field is associated with a lower strength index. The

inverse proportionality to strength index observed for COTTS, COTTL, and COTTG results because smaller differences in strength between the WP material and the upper layering cause weaker rarefactions. For case COTTG, the strength of the upper layers raised to that of WP material resulted in a reduced rarefaction and good residual stress field. The same relative effect of strength occurs when the upper layers and WP material are combined with the PZ surface only. For example, in COTTZ where the WP strength is reduced to near that of the upper layers, the combination of the rarefaction off the upper layers and the compressive reflection from the PZ surface still gives rise to a fairly good residual stress field. However, increasing the WP strength even slightly enhances the resulting rarefaction sufficiently to cause poor residual stress fields (i.e., COTTH, COTTF, and COTTX). For the baseline case COTTR, the influence of the strong rarefaction from the upper layer is sufficiently counteracted by the action of the shear-rarefaction motion induced by the weak colluvial layer on top of the PZ to give a fairly good residual stress field, as seen in Figure 6.

It is of interest to note that while many of the calculations show the general lack of a good residual stress field, none of them showed any tensile induced permeable connection from the WP region to the surface. In the numerical simulation of the BANEBERRY event [6], both a severe reduction of residual stresses below the cavity pressure and an induced tensile failure path from the WP to the surface were calculated. This combination represented a scenario of the venting of cavity gases that occurred on the BANEBERRY event. For the cases considered here, aside from the spall tensile region associated with reflection of shock wave at the surface, calculated tensile failure was only apparent below the cavity near the PZ surface.

CONCLUSIONS AND RECOMMENDATIONS

The present work discusses the rationale and highlights the results of a suite of calculations in support of a containment evaluation for an event having certain conditions marginally near the norm of experience. The calculations address the phenomena of the nuclear explosion induced shockwave

interacting with layering in close proximity (i.e. above and/or below) to the WP. Specifically, reflected disturbances from nearby layering propagating back into the residual stress regions are seen to significantly impair the development of the residual stress field. The calculated results indicate that degradation of the residual stress field is sensitive in a complex way on the layering and shear strength as illustrated by the following features:

- reflections from layering cause non-radial motion in the residual stress region.
- the degree of non-radial motion is dependent on the type of layering, proximity of the layering to the WP, and layer strength relative to that of the WP material.
- considerable degradation to the residual stress field can occur if the amplitude of non-radial motion is sufficiently high and its arrival coincides with the rebound process.
- for the baseline configuration studied, the weak thin colluvial layer above the PZ significantly reduces the non-radial motion induced by the rarefaction off the upper layers resulting in less degradation to the residual stress field.
- a stronger residual stress field results if the strength of the upper layers is increased relative to the WP material strength.
- a stronger residual stress field is obtained by reducing the WP strength relative to the strength of the upper layers.

The scope of the present suite of calculations is insufficient to ascertain a general quantitative effect of layering on residual stresses. Because it is essential to increase our understanding of layering effects in decisions affecting containment reliability, it is recommended that a general study using simpler layered geology be performed. Such a study would provide information to develop a scaling relationship indicating when reflections from layering could severely impair the residual stress field. For complex sites, numerical simulations are instructive in examining phenomena, but may not provide definitive decision making information for assessing containment reliability. In this context, effort should be made to develop additional

calculational criteria for the probability of successful containment other than having to rely on the concept of a strong, sufficiently thick residual stress field. Finally, because strength is the dominant material parameter affecting residual stresses, effort should be maintained to find a technique that will provide determination of insitu strength.

ACKNOWLEDGMENTS

The authors wish to acknowledge Larry Schwartz for his continued interest and support of the containment calculations, and to Miriam Lohmann for her service in the running and post-processing of the many and timely computer calculations. We extend appreciation to F. Heuze and C. Olsen for their review of this paper. We wish to thank Lydia Grabowski for her excellent typing and assistance in completing this paper.

This work was performed under the auspices of the U.S. Department of Energy by Lawrence Livermore National Laboratory under contract number W-7405-ENG-48.

REFERENCES

1. Burton, D.E., Lettis, L.A., Bryan, J.B., Frary, N., "Physics and Numerics of the TENSOR Code," Lawrence Livermore National Laboratory, Livermore, CA, UCID-19428 (1982).

2. Terhune, R.W. "Analysis of Burial Depth Criteria for Containment," Lawrence Livermore National Laboratory, Livermore, CA, UCRL-52395 (1978).

3. Nagy, G., and Florence, A.L., "Laboratory Investigation of Containment of Underground Explosions," SRI International, Menlo Park, CA, Bimonthly Progress Report PYU-8321 (20 Feb.-20 April 1985).

4. Rapp, E.G., "Containment of Buried Nuclear Explosions," Lawrence Livermore National Laboratory, Livermore, CA., UCRL-50604 (1968).

5. "Proc. Monterey Containment Symp., Monterey, CA, 1981, compiled by B.C. Hudson, E. M. Jones, C.E. Keller, and C. W. Smith (Los Alamos National Laboratory, Los Alamos, NM, 1981).

6. "Proc. 2nd Symp. Containment Underground Nucl. Exp.", Kirtland AFB, Albuquerque, NM, 1983, compiled by C.W. Olsen (Lawrence Livermore National Laboratory, Livermore, CA 1983).

7. Terhune, R.W., Glenn, H.D., Burton, D.E., McKague, H.L., and Rambo, J.T., "Calculational Examination of the Baneberry Event," Lawrence Livermore National Laboratory, Livermore, CA, UCRL-52365 (1977).

8. Butkovich, T.R., "The Gas Equation of State for Natural Materials," Lawrence Livermore National Laboratory, Livermore, Ca, UCRL-14729 (1967).

9. Schroeder, R.C., "A Comparison of Initial Conditions for Nuclear Explosion Calculations," Lawrence Livermore National Laboratory, Livermore, CA, UCRL-51671 (1974).

10. Anderson, G.D. and Kusubov, A.S., "Static and Dynamic Mechanical Properties Tests of Core Material from Hole U8j at the Nevada Test Site," Proc. of 3rd Symposium on Containment of Underground Nuclear Explosions, Idaho Falls, Idaho, (Sept. 9-13, 1985), also Lawrence Livermore National Laboratory, Livermore, CA, UCRL-92456 (1985).

11. Waggoner, J.L., and Howard, N.W., "U8j Preliminary Site Characteristics Summary," Lawrence Livermore National Laboratory, Livermore, CA, CP84-117, (November 2, 1984).

12. Terhune, R.W., and Glenn, H.D., "Estimate of Earth Media Shear Strength at the Nevada Test Site," Lawrence Livermore National Laboratory, Livermore, CA, UCRL-52358 (1977).

13. Rambo, J.T., and Bryan, J.B., "Calculation of High Surface Velocity Due to Focusing in the TYBO Event," Proc. Second Symposium on Containment of Underground Nuclear Explosions, Ed. C. W. Olsen, Kirtland AFB, Albuquerque, NM.

14. Swift, R.P., and Bryan, J.B., "Calculation of SRI Small-Scale PETN Grout-Clay-Granite Experiment," Presentation to the Executive Session of the Containment Evaluation Panel, S-Cubed, LaJolla, CA, (January 9, 1985).

15. Fogel, M.B., Private communication regarding letter to C. Keller, DNA/Field Command, from Pacifica Technology, Number PT-U-84-0670, 20 pages, (September 18, 1984).

Table 1 Baseline material properties for calculations representing U8j.

Material #	Hole Contact Depth Metres	Axis Range Metres	H_2O^M WT%	$\rho_o{}^M$ Mg/m^3	$\rho_g{}^M$ Mg/m^3	ϕ^C %	S^C %	ψ^C %	Poisson's Ratio	Velocity^M m/sec	P_T MPa	Max. Shear St. MPa	Unconfined Compressive Strength (MPa)
Alluvium 36 (Qtma)	0 - 127.9	320 413.16	6.9	2.13	2.66	25.7	57.3	11.0	0.20	1373	11.0	9.0	8.25
Rainier Mesa & Painthrush tuff 41 (Tgr+Tp)	None	413.1 372.0	11.4^F	1.69^F	2.48^F	39.7	48.8	20.3	0.20	1881^F	6.8	5.5	5.1
Grouse Canyon tuff 35 (Tbg)	127.9 165.9	372.0 338.1	20.0	1.33	2.49	57.1	46.7	30.4	0.15	1573	1.5	2.0	1.1
Tunnel Beds tuff 33 (Ttb)	165.9 379.9	338.1 118.2	15.5	1.67	1.51	44.0	58.7	18.2	0.20	1775	6.8	5.5	5.1
Red Rock Valley tuff 32 (Trb)	379.9 422.9	118.2 93.7	6.62	1.79	2.62	36.3	32.7	24.4	0.20	2207	6.0	6.0	4.8
Painthrush tuff 31 (Tp)	422.9 437.9	93.7 79.6	13.9	1.87	2.62	38.7	67.4	12.6	0.20	2219	7.0	170.0	5.19^M
Fraction Tuff MP material 30 (Tf)	437.9 574.1	79.6 -51.6	17.7	1.91	2.59	39.2	86.3	5.4	0.25	2338	9.1	50.0	4.69^M
Undifferentiated tuff (unsat.) 57 (Tu)	574.1	-51.6 -80.6	16.	1.95	2.65	38.1	81.7	7.0	0.25	2280	2.5	3.0	2.5
Undifferentiated tuff (sat.) 58 (Tu)	574.1 604.9	-51.6 -80.6	16.	1.95	2.65	42.4	100	0	0.25	2280	2.5	3.0	2.5
Paleozoic 60 (Pz)	604.9 2220	-80.6 -1700	2.0	2.7	2.8		100	0	0.20	6000	60.0	123.0	75.0

M = Measured values at U8j
F = Measured values at U8m
C = Calculated from measured values
ρ_o = Bulk density in Mg/m^3
ρ_g = Grain density in Mg/m^3
ϕ = Total porosity
ψ = Air filled porosity
S = Saturation
P_T = Elastic compression mean stress in MPa
Shear strength $=(\sigma_2 - \sigma_1)/2$

TABLE 2. Equivalent Shear Strengths for Fraction Tuff WP Material.

Hole	Event	K Value[1]	Distance WP to PZ,m	Strength[2] Index, MPa
8m	FRISCO	68	164	17.2
10T	SHUFFLE	59[3]	12.8	32.5[3]
3cn	BILBY	61	152.7	39.5[4]

FRISCO Calculation K = 69.4

1. $K = R_c (\rho h^{1/4}/W^{1/3})$ where Rc = cavity radius, W = yield, ρ = density, h = DOB. Average CEP K value is 70.2.
2. Based on Terhune method of calculating shear strength from cavity radii using cube root scaling formula. Strength = $(\sigma_2-\sigma_1)/2$
3. Assumed 1.8 Mg/m^3 overburden density.
4. Assumed 1.8 Mg/m^3 working point density.

Table 3. Summary of Calculational Results

Case	Cavity Press MPa	Cavity Radius m	Strength[1] Index MPa	Rebound time, s Calc.	Rebound time, s Model[2]	Residual[3] stresses Tang[4]	Residual[3] stresses Hoop[5]	Rank of Stress Field
Uniform Geology								
COTTU	19.9	54.39	19.48	.208	.212	High	High	1
Baseline Geology								
COTTR	15.0	58.15	14.65	.275	.244	Marginal	Marginal	5
COTTW	16.9	56.54	16.55	.259	.230	Marginal	Marginal	6
Upper Layers Only (upper layer strength varied)								
COTTS	17.2	56.30	16.85	.224	.228	Low	Low	12
COTTL	17.7	55.85	17.40	.222	.224	Low	Marginal	10
COTTG	18.2	55.56	17.83	.219	.222	Marginal	High	2
Lower Layers Only								
COTTT	17.8	55.83	17.45	.240	.224	Marginal	High	3
COTTK	21.2	53.57	20.70	.207	.206	Low	High	7
Upper Layers and PZ Surface (WP strength varied)								
COTTZ	11.6	61.80	11.10	.307	.280	High	Marginal	4
COTTH	13.4	59.73	12.98	.277	.259	Marginal	Low	8
COTTF	15.4	57.79	15.05	.255	.241	Marginal	Low	9
COTTX	18.3	55.48	17.94	.218	.221	Low	Low	11

1. Shear strength index based on Terhune's cube root scaling model.

2. Horizontal rebound time onset based on Terhune's cube root scaling model.

3. High = well above cavity pressure; Marginal = slightly above cavity pressure; Low = equal to or below cavity pressure.

4. Tang: tangential stress in-plane component ($\sigma_{\theta\theta}$)

5. Hoop: hoop stress is out-of-plane component ($\sigma_{\phi\phi}$)

Table 4. Summary of Non-Radial Motion Effects.

Case	Peak Non-Radial Motion,M/S	$(T_R-T_P)^1$,S	$(Z-Z_R)^2$,M	Rank of Stress Field
Uniform Geology				
COTTU	3.1	-.017	0.14	1
Baseline Geology				
COTTR	3.3/4.0	.155/-.055	0.14	5
COTTW	5.2	.079	0.25	6
Upper Layers (upper layer strength varied)				
COTTS	8.6	-.021	0.51	12
COTTL	7.65	-.020	0.45	10
COTTG	7.05	-.020	0.23	2
Lower Layers				
COTTT	2.2/3.6	.120/.02	0.10	3
COTTK	5.1/-2.0	.042/-.073	0.12	7
Upper Layers and PZ Surface (WP strength varied)				
COTTZ	8.1	.082	0.11	4
COTTH	8.6	.067	0.18	8
COTTF	8.8	.055	0.22	9
COTTX	9.0	.020	0.44	11

1. Time between rebound onset and peak non-radial motion.

2. Additional non-radial displacement after rebound onset.

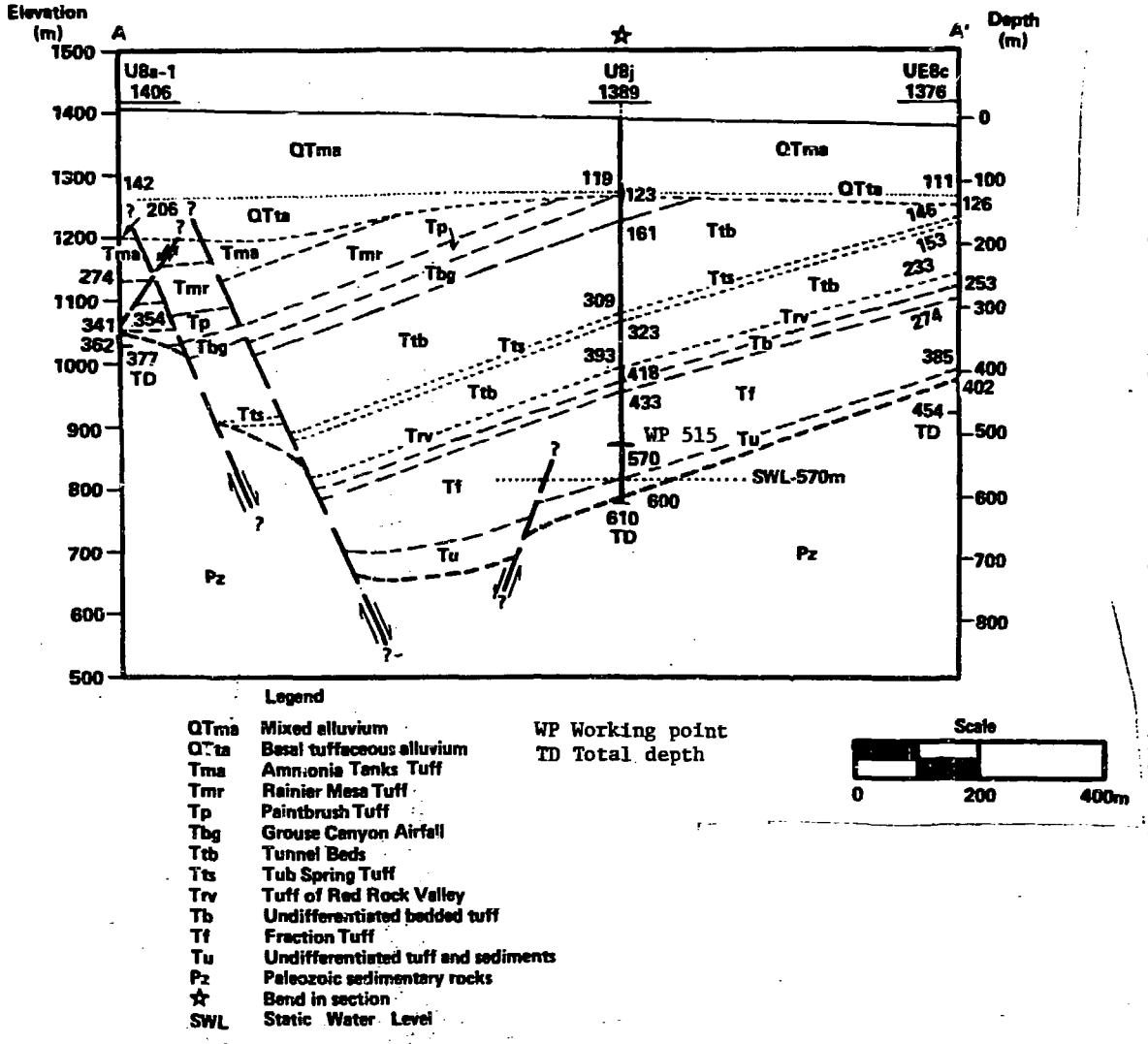

Figure 1 East-West geologic cross-section for U8j, from Ref. 11.

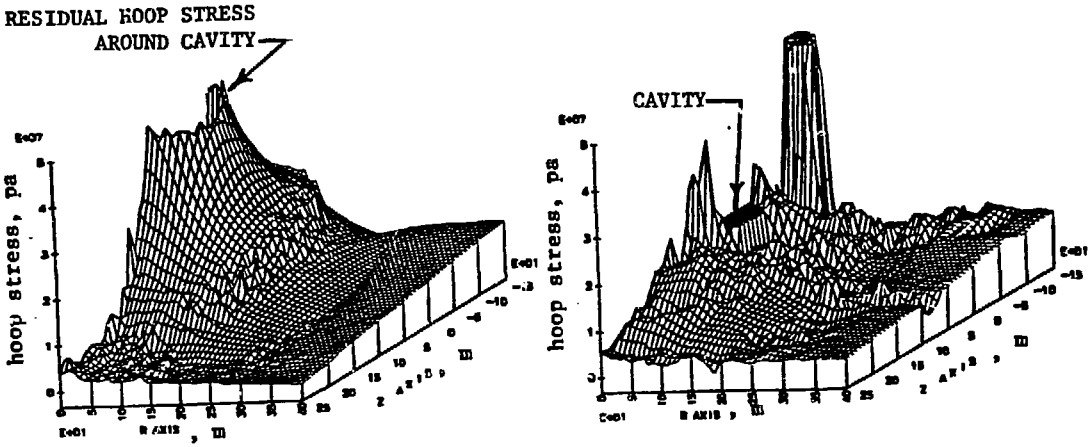

(a) no layering

(b) layering

Figure 2 Examples of residual hoop stress a) uniform geology, no layering b) layering above and below WP.

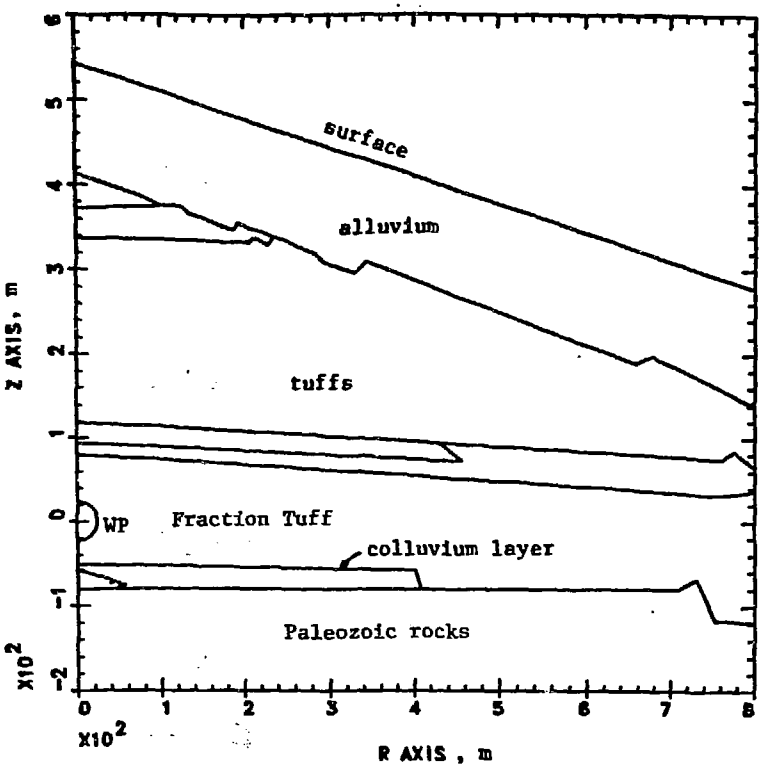

Figure 3. Calculational configuration for baseline geology of U8j

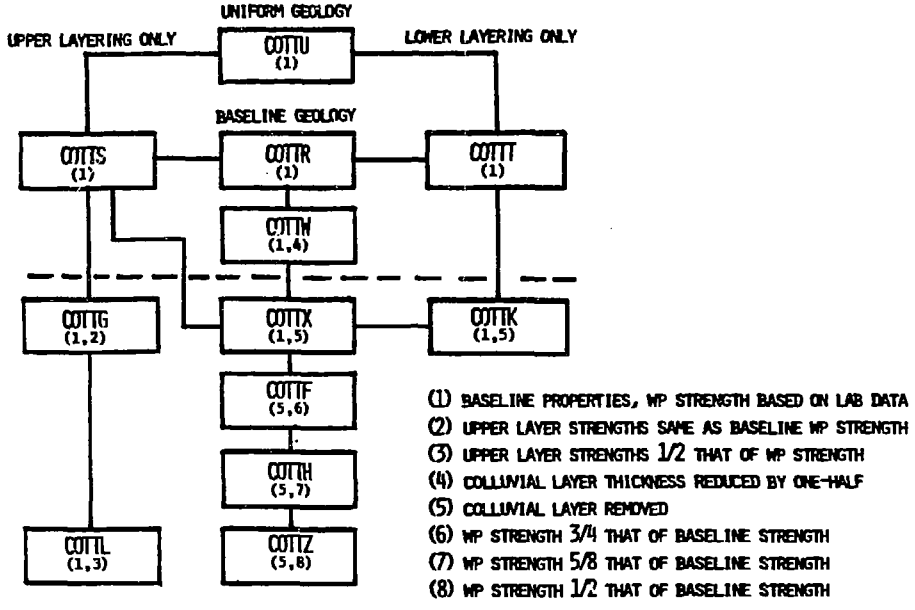

Figure 4 Diagram of TENSOR calculations.

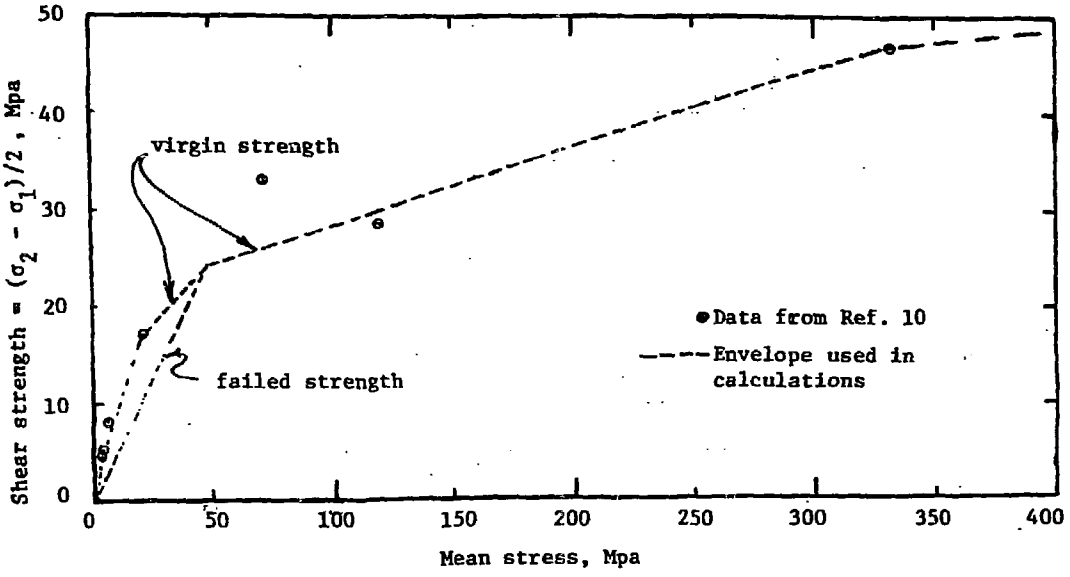

Figure 5 Triaxial compression strength measurements and strength used for Working point material. Core samples from a depth of 493.78m in U8j

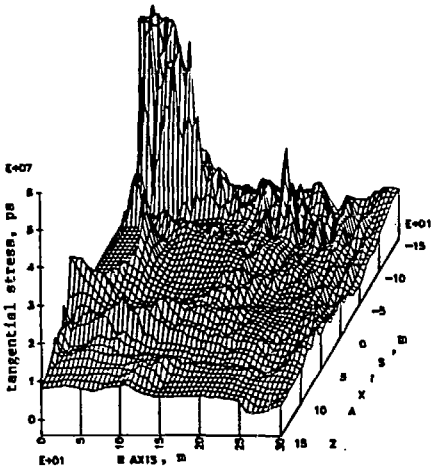

(a) tangential stress

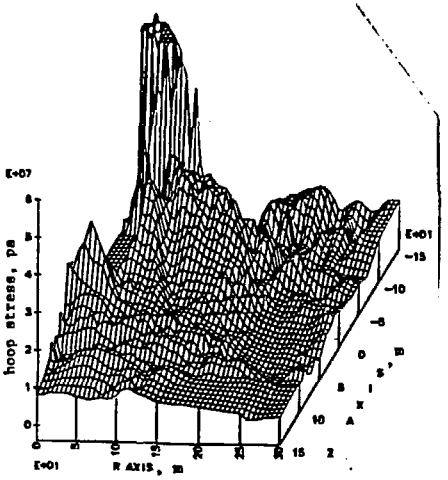

(b) hoop stress

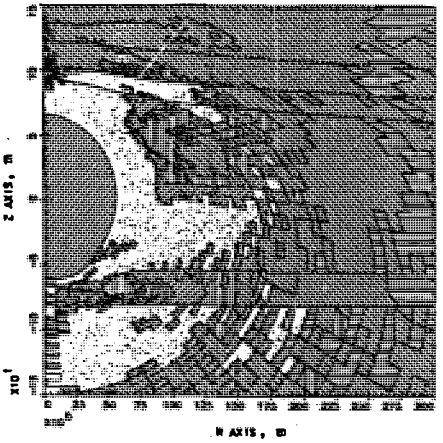

(c) tangential stress

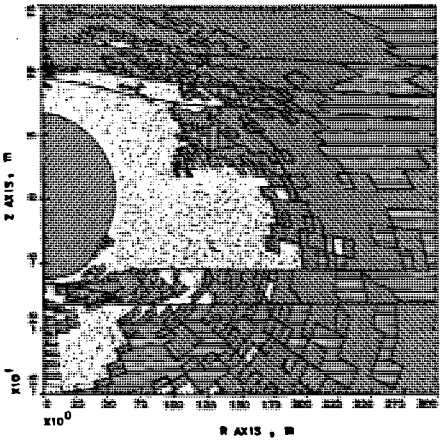

(d) hoop stress

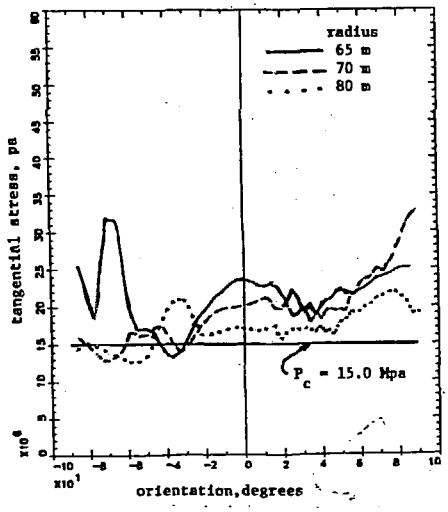

(e) tangential stress

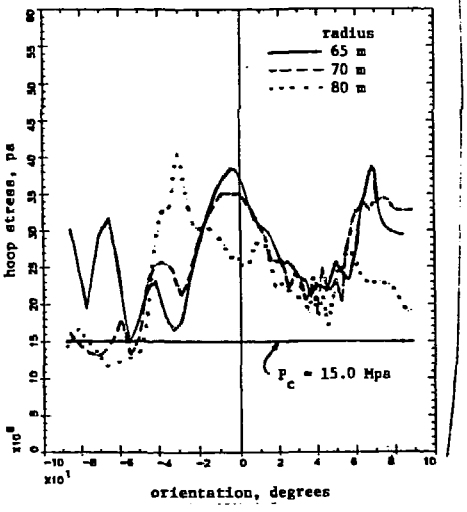

(f) hoop stress

Figure 6 Residual stresses for baseline case COTTR with colluvial layer.

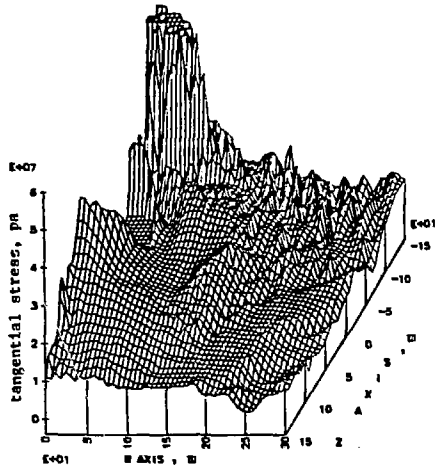

(a) tangential stress

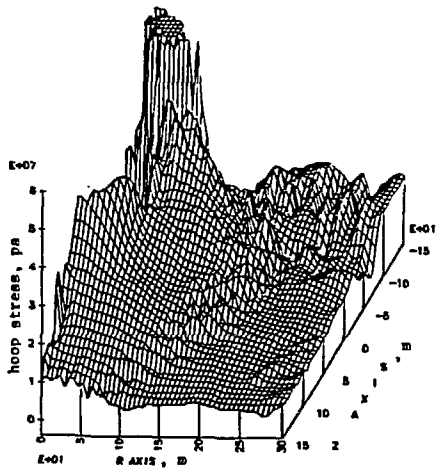

(b) hoop stress

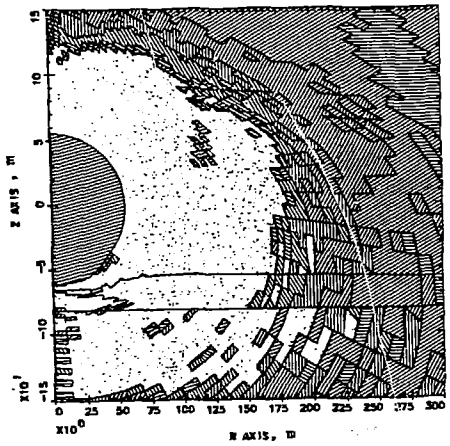

(c) tangential stress

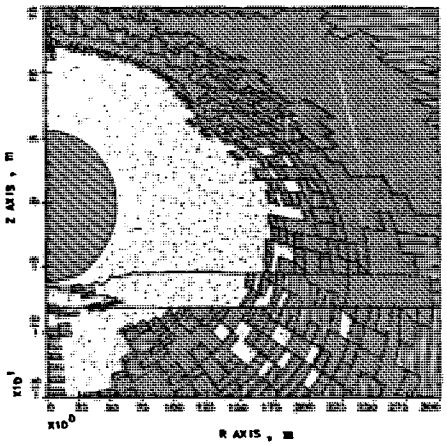

(d) hoop stress

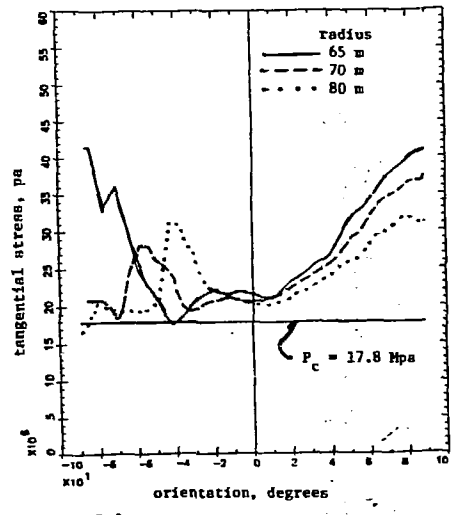

(e) tangential stress

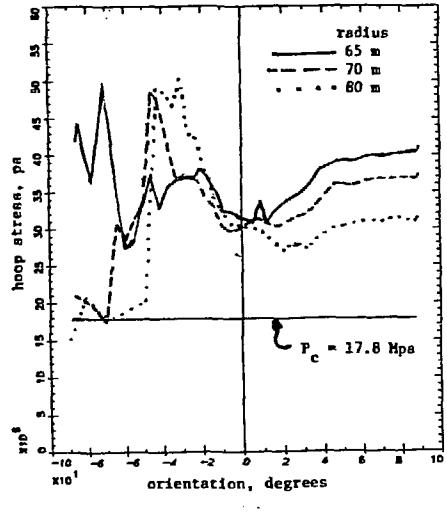

(f) hoop stress

Figure 7 Residual stresses for lower layering case COTTT with colluvial layer.

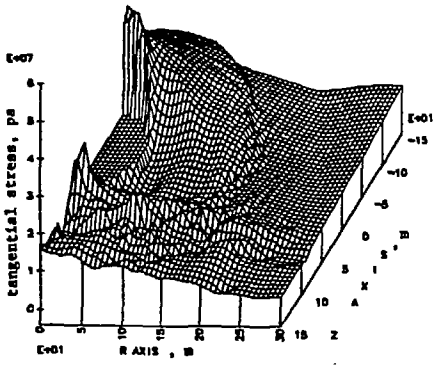

(a) tangential stress

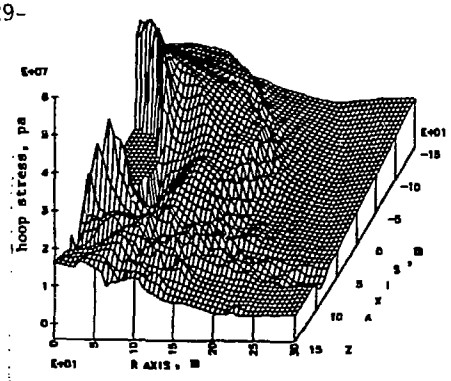

(b) hoop stress

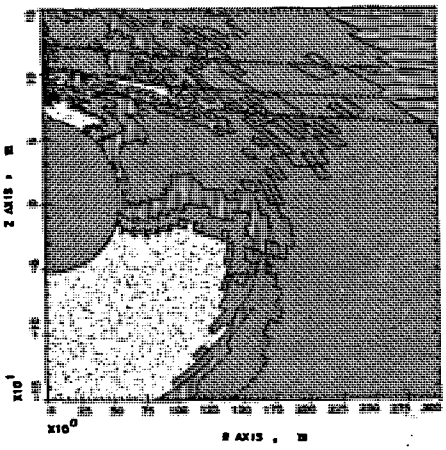

(c) tangential stress

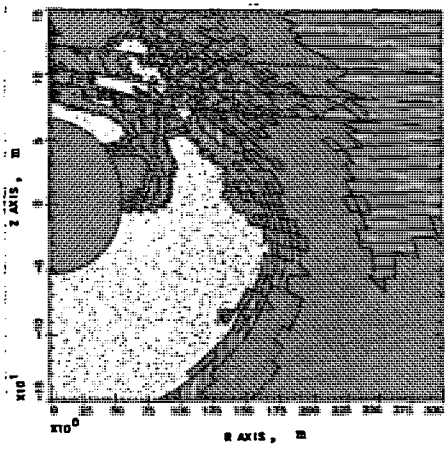

(d) hoop stress

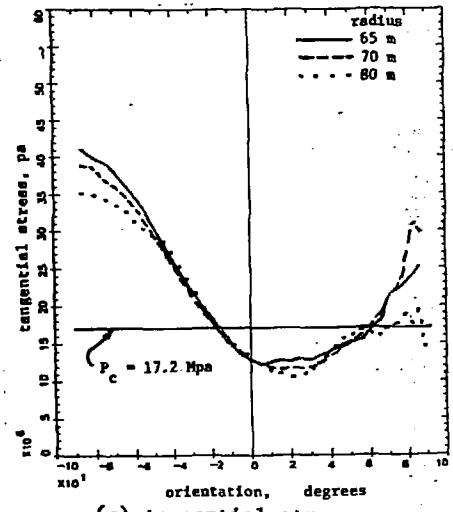

(e) tangential stress

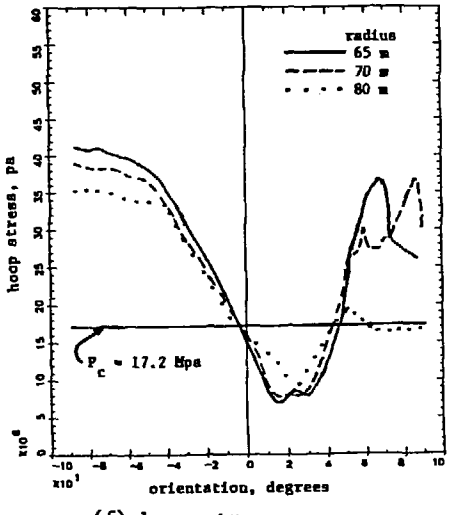

(f) hoop stress

Figure 8 Residual stresses for upper layering case COTTS.

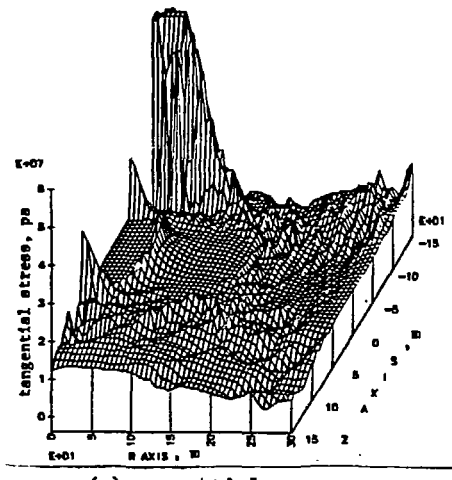

(a) tangential stress

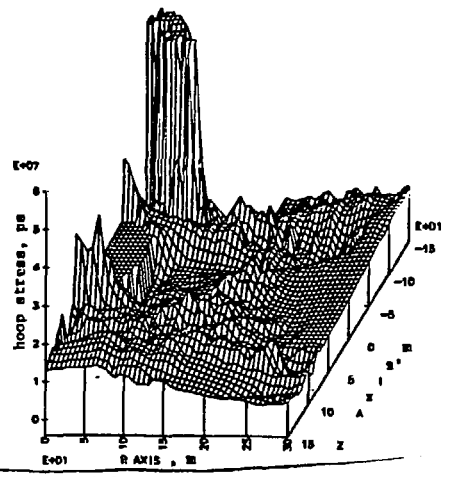

(b) hoop stress

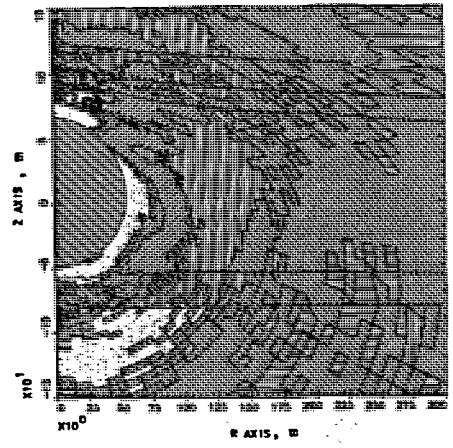

(c) tangential stress

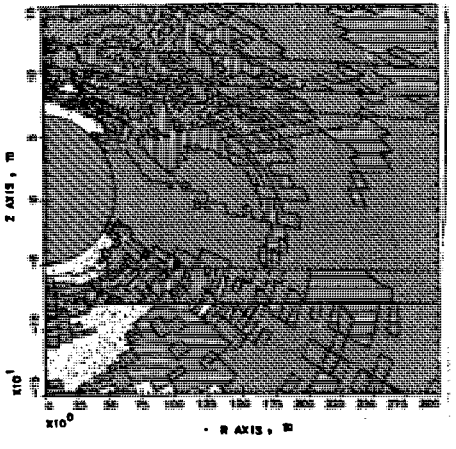

(d) hoop stress

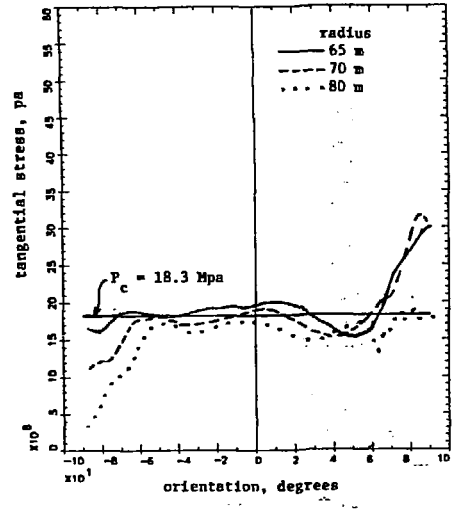

(e) tangential stress

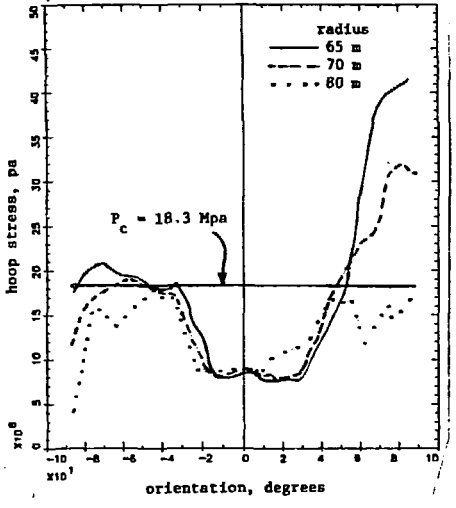

(f) hoop stress

Figure 9 Residual stresses for layered case COTTX without colluvial layer.

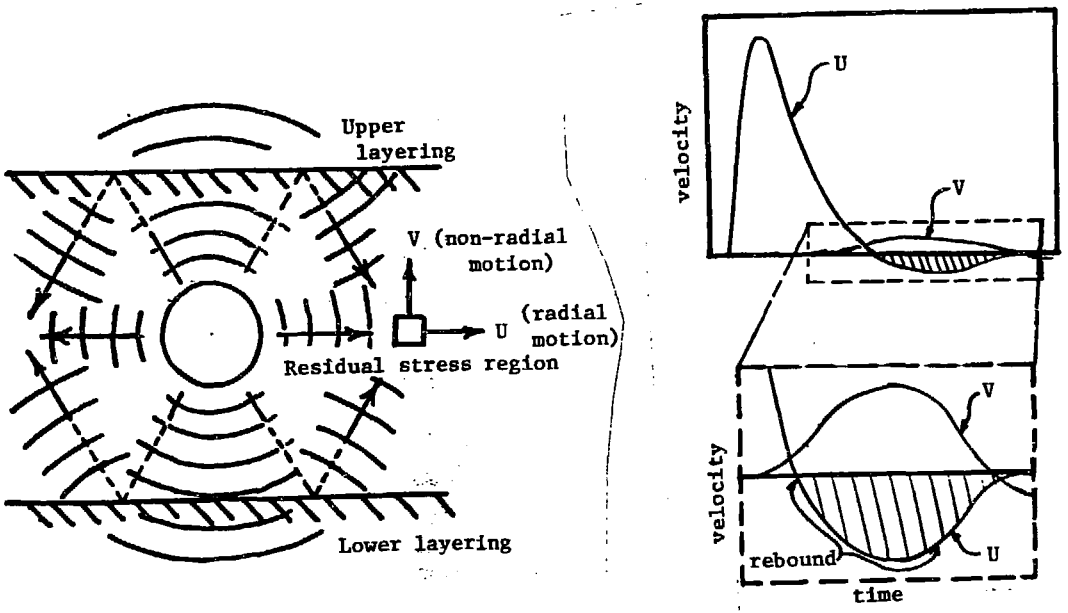

Figure 10 Illustration of layering-induced non-radial motion.

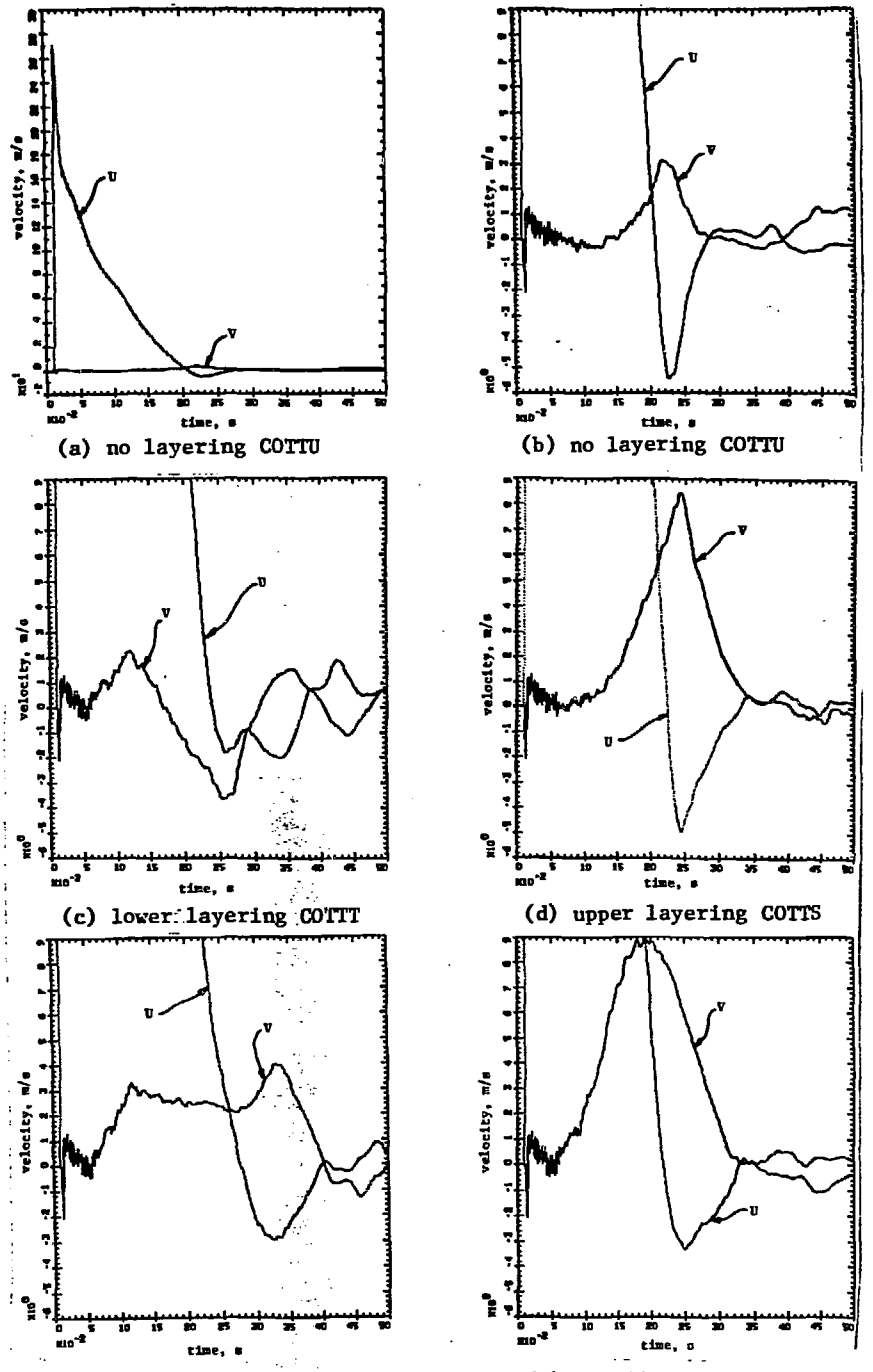

(a) no layering COTTU

(b) no layering COTTU

(c) lower layering COTTT

(d) upper layering COTTS

(e) baseline case with colluvial layer COTTR

(f) baseline case without colluvial layer COTTX

Figure 11 Examples of radial U and non-radial V velocity responses at WP level at a range of 50mm.

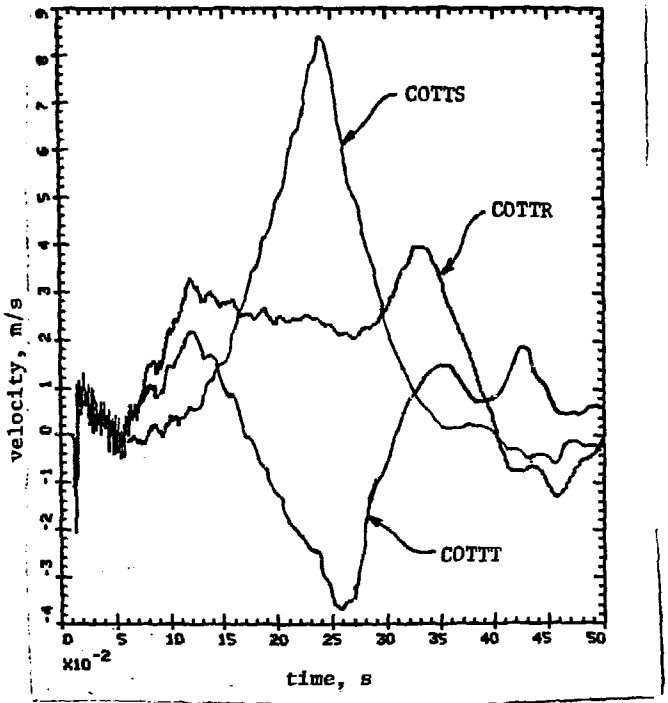

Figure 12 Non-radial velocity response at WP level and range of 50 m for case COTTR with colluvial layer along with contributing components from upper layering COTTS and lower layering COTTT.

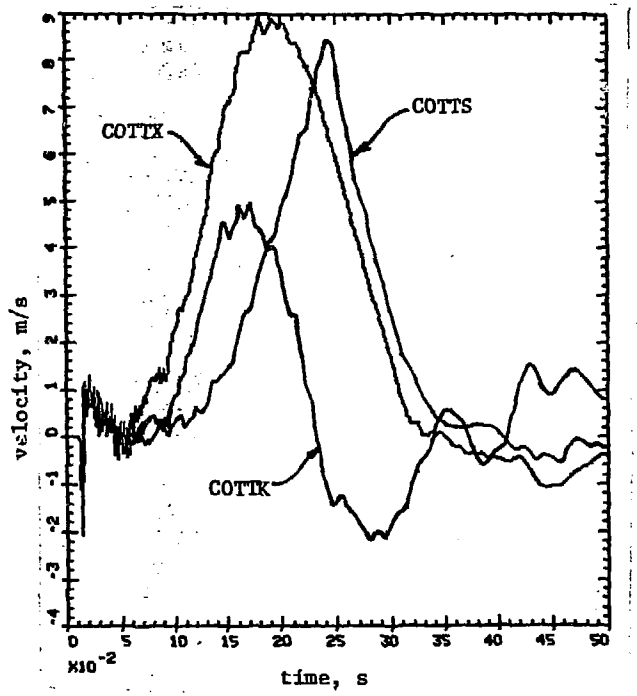

Figure 13 Non-radial velocity response at WP level and range of 50 m for case COTTX without colluvial layer along with contributing components from upper layering COTTS and PZ surface COTTK.